STRUCTURAL CHANGES IN FRICTION-STIR WELDED Al-Li-Cu-Sc-Zr (1460) ALLOY

Alla L. Berezina[1], Nataliya N. Budarina[1], Andriy V. Kotko[1], Oleg A. Molebny[1*], Alla A. Chayka[2], Alexander Ya. Ischenko[2]

1 G.V.Kurdiumov Institute for Metal Physics, National Academy of Sciences of Ukraine, Vernadsky Blvd. 36,03142, Kyiv, Ukraine
2 E.O.Paton Electric Welding Institute, National Academy of Sciences of Ukraine, Bozhenko Str. 11, 03680, Kyiv, Ukraine

ABSTRACT

Structure and properties of Al-2.3%Li-3%Cu-0.1%Sc-0.1%Zr (1460) were studied after FSW on thin cold-rolled sheets with the thickness of 2mm. Sheets were aged in the T8mode. During FSW, severe plastic deformation and material flow occurs at the temperature lower than melting temperature. Welding was performed at the tool rotation speed 2880 rps. The tool was moved along the weld joint at the constant speed 16m/h.

Key words: friction stir welding, Al-Li-Cu-Sc-Zr alloys, plastic deformation, recrystallization, structural evolution

INTRODUCTION

Friction stir welding (FSW) is a relatively new solid-state joining process. FSW and friction stir processing (FSP) are emerging as very effective solid-state joining/processing techniques. FSW was invented at the Welding Institute of UK in 1991 as a solid-state joining technique, and it was initially applied to aluminium alloys [1] (Thomas et al., 1991).During FSW the metal transforms to the special plasticized state (an analogue of non-Newtonian liquid) due to high-speed intense plastic deformation at high temperatures. FSW involves complex interactions among a variety of simultaneous thermo-mechanical processes. The interactions affect the heating and cooling rates, plastic deformation and flow, dynamic and post-dynamic recrystallization phenomena, as well as the mechanical integrity of the joint [2].

A unique feature of the friction-stir welding process is that the transport of heat is aided by the plastic flow of the substrate close to the rotating tool. The heat and mass transfer depends on material properties as well as welding variables including the rotational and welding speeds of the tool and its geometry. In FSW, the joining is produced by extrusion and forging of the metal at high strain rates. The effect of welding on microstructural evolutions and resulting joint properties have been investigated. Durometric, resistometric, X-ray and

* e-mail: moleb@imp.kiev.ua, tel: (+38)0444243210

electron-microscopy studies were performed on different weld zones: the stirred zone; the thermo-mechanically affected zone; the heat-affected zone; the base metal. The density and nature of dislocations, and average grain sizes in different weld zones were determined using X-ray diffraction peak profile analysis. Particular attention was given to the effect of post-weld ageing on the strength of the weld. Structural and durometric studies were performed after repeated aging.

METHODS OF SPECIMEN MANUFACTURING AND ANALYSIS

Structure and properties of Al-2.3%Li-3%Cu-0.1%Sc-0.1%Zr (commercial 1460 alloy) were studied after FSW on thin cold-rolled sheets 2mm thick. Sheets were aged in the T8 mode. During FSW, severe plastic deformation and material flow occurs at temperature lower than melting temperature. Welding was performed at the tool rotation speed of 2880rps. The tool was moved along the weld joint at the constant speed of 16m/h.

The cross-section of the FSW plate was cut in the middle along the plate length for the microstructural characterization.

Metallographic studies were carried out on polished and etched cross-section surface. Etching was done using Keller's reagent at room temperature. Four different etching zones were observed: A – stirred zone (SZ); B&C – thermo-mechanically affected zone (TMAZ); D – heat affected zone (HAZ) & base metal (BM). Location of HAZ can be estimated by hardness curve behavior.

The half–plate where the direction of tool rotation is the same as the direction of half-plate motion is called the *retreating* side (marked as C), with the other side designated as being the *advancing* side (marked as B). Extrusion phenomena were observed on the retreating side. This in itself proves that material flows from advancing to retreating side during FSW.

The phase structure as well as dislocations and grain sizes were observed in the base material and FSW sample using transmission electronic microscopy (TEM). Disc specimens (3mm in diameter) were prepared by mechanical grinding to 250μm thickness and electropolishing using a 30% nitric acid solution in methanol with 60Vx1A at –20ºC. Material for these specimens was taken from different weld zones at four different sites along the midthickness of the cross-section in FSW sample as marked with rectangles in *Fig.1*.

Resistance measurements were carried out using an experimental arrangement based on the classical four-probe d.c. method. Measurements were performed at the heating rate of 3ºC/min in the temperature range from room temperature to 600 ºC.

The X-ray diffraction profiles for the base material and FSW sample were measured by a HZG-1 diffractometer.

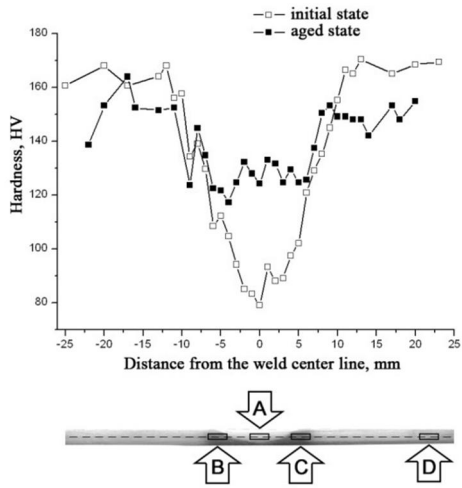

Fig. 1– Vicker's hardness plot scaled to the weld macrostructure picture

The radiation was CuK_α at operating parameters of 20 mA and 35 kV, and Al_2O_3 single crystal (standard) was used to separate the instrument broadening effects. The pseudo-Voigt analytical function plus the linear background were fitted to the overlapping peaks. Physical broadening was obtained by the Halder-Wagner relation $\beta_{phys} = \sqrt{\beta_{\exp}^2 - \beta_{\exp}\beta_{etalon}}$, where β is integral peak profile of experimental and standard peak profiles.

RESULTS AND DISCUSSION

The Vicker's hardness was measured on polished surfaces across the weld 1mm below the surface from the advancing to the retreating side from base metal to base metal (Fig. 1). Hardness data were obtained with a hardness meter, with the test load of 5kg and the load time of 20 s. Durometric study showed a 50% weakening in SZ after FSW and suggested a plausible hardening up to 75% of base metal hardness after aging in the T8 mode.

The following results were obtained by OM and TEM: texture and partial recrystallization were observed in the base metal zone. Nano-dispersed T_1-phase and nano-composite δ′/θ′, δ′/Al_3(Sc,Zr) particles [3] were present in the matrix. This resulted in alloy hardening. Complete recrystallization occurred in the stirred zone after FSW, the texture disappeared, grains became equiaxial, were of 1-3μm size, without substructure. θ′ and T_1 phases dissolved. There were only δ′ and δ′/Al_3(Sc,Zr) phases present in the stirred zone. The δ′ and δ′/Al_3(Sc,Zr) phases were only present in the stirred zone; hardness decreased.

Grain sizes in the thermo-mechanically affected zone remained constant. But the volume part of T_1 phase increased significantly and T_2 phase appeared on the T_1 phase – matrix interface. Anomalous grain growth up to 30 – 100 μm occurred in the heat-affected zone.

TEM results (*Fig. 2*) are in good agreement with metallographic and resistometric ones.

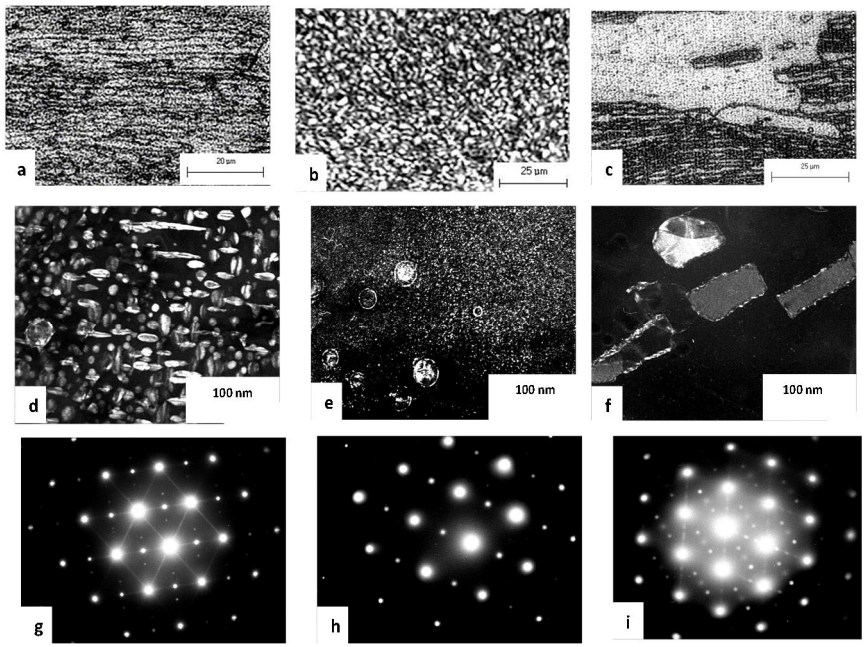

Fig. 2 – Metallographic and TEM studies: base metal: *a* – grain structure, *d* – phase structure, *g* – selected area diffraction pattern; stirred zone: *b* – grain structure, *e* – phase structure, *h* – selected area diffraction pattern; thermo-mechanically affected zone: *f* – phase structure, *i* – selected area diffraction pattern; heat-affected zone: c– grain structure

As one can see from the curves of changes in temperature coefficient of electrical resistivity (*Fig. 3*), two main temperature areas can be marked out on all curves: the positive peak at low temperatures caused by δ′ phase dissolution and the negative peak at high temperatures, which can be accounted for by T_1 phase formation. Small negative peak before δ′ phase dissolution peak on SZ sample curve proves that the material in SZ changed to solid solution state because of intensive

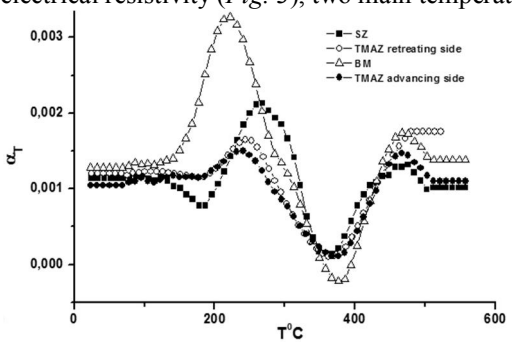

Fig. 3 – Changes in temperature coefficient of electrical resistivity α_T at continuous heating at the speed of 3ºC/min during 20-600ºC temperature range

plastic deformation during FSW.

X-ray diffraction analysis is known to be a useful technique for evaluating the microstructural characteristics such as dislocation density and size of the coherent scattering domains [4]. The presence of dislocations and small size of crystallites lead to X-ray diffraction peak profile broadening, which is used in methods of microstructural parameters estimation.

The Williamson-Hall plots [5] show the qualitative behavior of diffraction peak broadening with full width at half maximum (or integral breadths) as a function of K, where $K=2\sin\theta/\lambda$, θ and λ are the diffraction angle and the wavelength of X-ray radiation, respectively. Strain anisotropy in the conventional Willimson-Hall plot was rationalized by substituting $KC^{1/2}$ for K [6], which is now known as the Willimson-Hall-Ungar method.

Where anisotropy microdistortion resulted in anisotropic diffraction line broadening [7], Ungar added the dislocation contrast factor $\bar{C}$, which can be determined by elastic anisotropy and dislocation type of the material [8], to the known relation:

$$\Delta K \cong \frac{0.9}{D} + \left(\frac{\pi M^2 b^2}{2}\right)^{1/2} \rho^{1/2} K\sqrt{\bar{C}} + O(K^2\bar{C}) \quad \Delta K \cong \frac{0.9}{D} + \left(\frac{\pi M^2 b^2}{2}\right)^{1/2} \rho^{1/2} K\sqrt{\bar{C}} +$$

$$O(K^2\bar{C}) \quad \Delta K \cong \frac{0.9}{D} + \left(\frac{\pi M^2 b^2}{2}\right)^{1/2} \rho^{1/2} K\sqrt{\bar{C}} + O(K^2\bar{C}),$$

Where $K = 2\sin\theta/\lambda$ $K = 2\sin\theta/\lambda$, θ – diffraction angle, λ – X-ray wavelength, $\Delta K = \cos\theta[\Delta(2\theta)]/\lambda$ $\Delta K = \cos\theta[\Delta(2\theta)]/\lambda$, here $\Delta(2\theta)$ is the integral weight of diffraction peak, D – the average size of crystallites, M – the constant of effective outer cut-off radius of dislocation, ρ – the average dislocation density, b – Burgers module.

The average value of dislocation contrast factor is determined using elastic constants for Al, and constructed as a function of elastic constants for possible dislocations in face-centred cubic (f.c.c.) lattice.

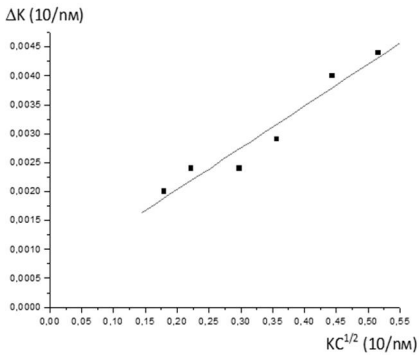

Fig. 4 – The Williamson-Hall-Ungar plot for base metal

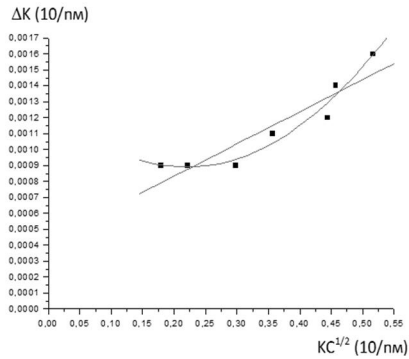

Fig. 5 – The Williamson-Hall-Ungar plot for stirred-nugget zone.

The Williamson-Hall-Ungar relations are shown in *Fig.4-6* for different states of materials. The Willimson-Hall-Ungar plot provides two important microstructural features in the material under investigation. First, the slope of the linear regression is proportional to the microstrain.

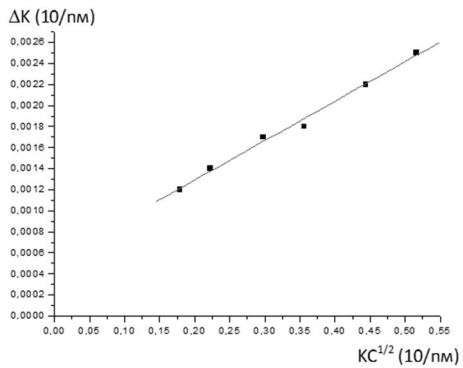

Fig. 6 – The Williamson-Hall-Ungar plot for TMAZ/HAZ

Second, the intercept of the linear regression with the data points at $K = 0$ is a rough size-estimation of the coherent scaterring domains indicating by the similar average crystallite size.

Such type of dislocation structure was proved to persist in all specimens. This is evidenced by the fact that the best linear regressions were achieved with elastic constant $c_{12}/c_{44} = 2$. It is to be noted that the Williamson-Hall-Ungar plot is parabolic for the stirred zone (*Fig. 5*). The average coherent domain size is 70.86 nm, which agrees with electronic microscopy data. It can be seen from *Table 1* that the largest distortions are present in the base material, and the smallest ones – in the stirred zone.

Calculation results of microstructural parameters are shown in *Table1* (R-factor is accuracy of regression):

Table 1

State	D, nm	ε	R-factor

Base metal	118.9	0.0077	0.96
Stirred zone	193.18 (linear regression)	0.0019	0.90
	70.86(parabolic regression)		0.96
NMAZ/HAZ	159.84	0.0037	0.99

CONCLUSIONS

It is possible to conclude relying on the data obtained that:

- the base alloy is non-recrystallized, textured, with banded grain structure, there are highest internal strains (Table 1) observed, work-hardening takes place due to composite phases δ′/θ′ , δ′/Al_3(SC,Zr) and triple T_1 phase;

- there is complete recrystallization with dissolution of δ′/Al_3(SC,Zr) phases and T_1 phase observed in the stirred zone, complete relaxation of strains with the formation of equiaxial grains of 2-3 μm size. There are both composite δ′/Al_3(SC,Zr) phase particles and fine-dispersed homogeneous δ′ phase particles present in the matrix;

- there are internal strains in the thermo-mechanically affected zone, grains are equiaxial of 2-3 μm size, there is mainly rough T_1 phase present in the matrix and T_2 phase emerged on the T_1 phase – matrix interface;

- the areas of anomalous grains growth appear in the heat-affected zone.

REFERENCES

[1] Thomas, W.M., Nicholas, E.D., Needham, J.C., Murch, M.G., Templesmith, P., Dawes, C.J., 1991. G.B. Patent Application 9125978.8.
[2] R. Nandan, T. DebRoy and H. K. D. H. Bhadeshia. Progress in Materials Science 53 (2008) 980-1023
[3] I.N.Fridlander, K.V.Chuistov, A.L.Berezina, N.N.Kolobnev. Aluminium-lithium alloys. Structure and properties. Naukova dumka. Kyiv. 1992
[4] M.A.Krivoglaz. Theory of X-ray and Thermal Neutron Scattering by Real Crystals. Plenum Press. New York. 1996
[5] G.K.Williamson, W.H.Hall, ActaMetall. 1 (1953) 22
[6] T.Ungar, A.Borbely. Appl.Phys.Lett 69 (1996) 3173
[7] G.Caglioti, A.Paoletti, F.P.Ricci, Nucl. Instrum. 3 (1958) 223
[8] T.Ungar, I. Dragomir, A.Revesz, A.Borbely, J.Appl. Cryst. (1999) 32, 992